

Radiative Transfer Analysis of Far-UV Background Observations Obtained with the Far-Ultraviolet Space Telescope (FAUST)

Adolf N. Witt, Brian C. Friedmann

Ritter Astrophysical Research Center, University of Toledo, Toledo, OH 43606

and

Timothy P. Sasseen

Center for EUV Astrophysics,

2150 Kittredge Street, University of California, Berkeley, CA 94720

ABSTRACT

In 1992 the Far-Ultraviolet Space Telescope (FAUST) provided measurements of the ultraviolet (140-180nm) diffuse sky background at high, medium, and low Galactic latitudes. A significant fraction of the detected radiation was found to be of Galactic origin, resulting from scattering by dust in the diffuse interstellar medium. To simulate the radiative transfer in the Galaxy, we employed a Monte Carlo model which utilized a realistic, non-isotropic radiation field based on the measured fluxes (at 156nm) and positions of 58,000 TD-1 stars, and a cloud structure for the interstellar medium. The comparison of the model predictions with the observations led to a separation of the Galactic scattered radiation from an approximately constant background, attributed to airglow and extragalactic radiation, and to a well constrained determination of the dust scattering properties. The derived dust albedo $a = 0.45 \pm 0.05$ is substantially lower than albedos derived for dust in dense reflection nebulae and star-forming regions, while the phase function asymmetry $g = 0.68 \pm 0.10$ is indicative of a strongly forward directed phase function. We show the highly non-isotropic phase function to be responsible, in conjunction with the non-isotropic UV radiation field, for the wide range of observed correlations between the diffusely scattered Galactic radiation and the column densities of neutral atomic hydrogen. The low dust albedo is attributed to a size distribution of grains in the diffuse medium with average sizes smaller than those in dense reflection nebulae.

Subject headings: radiative transfer — scattering — ultraviolet: ISM

1. Introduction

When illuminated by the galactic interstellar radiation field, dust in the interstellar medium gives rise to scattered radiation known as diffuse galactic light (DGL). Efforts to observe the DGL at different wavelengths and attempts to derive scattering properties of the dust grains from such data have extended over the past half-century, and corresponding work directed at the far-ultraviolet spectral region has been ongoing during the past quarter-century. A detailed review of DGL studies was given by Witt (1990), while Bowyer (1991) and Henry (1991) reviewed in-depth the particular complications involved in the observation and interpretation of the far-ultraviolet background radiation due to several sources, including the DGL.

Major challenges facing DGL studies in the far-ultraviolet include the need for observations with high diffuse-source sensitivity which provide extensive sky coverage while simultaneously offering the means to separate the flux from discrete sources, such as stars and galaxies, from that of the diffuse background. For the interpretation of DGL data, there has been a demand (Mathis 1993) for multiple-scattering models which take into account the inhomogeneity of the scattering interstellar medium and the anisotropic distribution of the interstellar radiation field, which is extreme for the far-ultraviolet sky (Murthy & Henry 1995). The successful flight of the Far-Ultraviolet Space Telescope (FAUST) (Bowyer et al. 1993), conducted as part of NASA's 1992 ATLAS-1 shuttle mission (Craven & Torr 1988), has been a response to the first of these two challenges. The photon-counting imaging detector of FAUST (Lampton et al. 1990) allowed a separation of the diffuse background from that due to stars in the field to a level where unresolved stars contribute less than one percent of the total diffuse intensity in the field (Cohen et al. 1994). At the same time, this instrument provided sensitive measurements of the diffuse background in fields covering over 1000 square degrees in representative directions ranging from high to intermediate latitudes (Sasseen et al. 1995). Sasseen et al. (1995) showed that the dominant component in the measured far-ultraviolet background is due to starlight scattered by galactic dust by demonstrating a clear relationship between spatial power spectra of the IRAS 100 μ m cirrus and the FAUST far-ultraviolet diffuse background images.

An initial attempt to model the FAUST ultraviolet background and to constrain the scattering properties of the diffusely distributed dust was undertaken by Sasseen & Deharveng (1996). This attempt, which used the simple model of Jura (1979) for high-latitude dust illuminated by a constant plane source, met with only limited success however. The model was unable to correctly reflect the anisotropy and the longitudinal variation of the intensity of the illuminating radiation field.

In this paper, we are using a substantially more sophisticated model to treat the

radiative transfer for the diffuse background regions observed by FAUST. This model was first introduced and described briefly by Witt & Petersohn (1994, hereafter WP) in the context of an analysis of ultraviolet background observations made by the Dynamics Explorer 1 spacecraft (Fix et al. 1989).

The organization of this paper is as follows. In §2 we will summarize the data reduction and present an initial analysis. This will establish that the measured intensities are a combination of DGL, which is dependent on the column density of the dust in the line of sight, and of roughly constant contributions from airglow and possible extragalactic diffuse background radiation. In §3 we will present the WP model in greater detail than was done in WP (1994). Following this, we carry out the radiative transfer analysis of the FAUST data in §4, followed by a discussion of the implications of the derived dust properties for the likely processing of interstellar dust in the diffuse medium away from the galactic plane in §5. In §6 we will summarize our results and formulate our conclusions.

2. The Data

The data used for this analysis were obtained with the imaging telescope, FAUST, during a March 1992 shuttle flight. FAUST has a bandpass covering the range 140 - 180nm and a 7.6° circular field of view. The detector was a photon-counting microchannel plate with a wedge-and-strip position sensitive anode (Lampton et al. 1986). The in-flight angular resolution of the all-reflecting camera (D=161mm, f/1.12) was approximately 3.8', which permitted the identification and removal of point sources down to a detection limit of 1×10^{-14} erg s⁻¹ cm⁻² Å⁻¹. Each pixel found to contain excess flux due to a point source was replaced with a weighted average based on distance, of those surrounding pixels containing negligible flux from the source (Sasseen et al. 1995).

A summary of the data used for this analysis is given in Table 1. The list contains the same FAUST fields as studied by Sasseen & Deharveng (1996), to which we have added data from the FAUST image # 2 in Dorado. The columns in Table 1 give, respectively, (1) the name of the FAUST field (Sasseen & Deharveng 1996); (2) the FAUST image number (Bowyer et al. 1993); (3) the number of 0.5° x 0.5° pixels in each image for which the diffuse UV intensity was determined; (4) & (5) the galactic coordinates for the image center, (6) the average intensity of the diffuse radiation in the 140-180nm FAUST band in units of photons cm⁻² s⁻¹ Å⁻¹ sr⁻¹, (hereafter referred to as "units"); (7) the average intensity of the diffuse IRAS background radiation at 100μm (IPAC 1991); and (8) the average HI column density taken from the Bell Lab HI Survey (Stark et al. 1992), supplemented with data from the Parkes HI survey (Cleary et al. 1979; Heiles & Cleary 1979) for declination

Table 1. Data Used in this Study

FAUST Field	#	Points	ℓ	b	$\langle I(\text{UV}) \rangle$	$\langle I(100\mu\text{m}) \rangle$	$\langle N(\text{HI}) \rangle$
(1)	(2)	(3)	($^\circ$)	($^\circ$)	(PU)	(MJy/sr)	($10^{18}/\text{cm}^2$)
			(4)	(5)	(6)	(7)	(8)
Dorado	2	49	266.2	-44.4	1705 \pm 90	0.272 \pm 0.227	200.8 \pm 55.1
NGPKM	8	64	250.1	76.3	900 \pm 56	2.055 \pm 0.435	261.5 \pm 17.5
M87	9	64	285.5	75.0	1431 \pm 75	2.389 \pm 0.367	242.8 \pm 17.8
Virgo P2	10	58	284.3	76.4	1023 \pm 51	2.255 \pm 0.445	245.5 \pm 18.0
Virgo P1	11	62	283.8	71.6	1052 \pm 137	2.315 \pm 0.241	191.6 \pm 29.8
Centaurus	14	59	302.8	21.7	3169 \pm 174	8.624 \pm 1.104	747.1 \pm 76.0
M83	16	64	314.7	32.8	1777 \pm 147	4.878 \pm 0.536	446.0 \pm 52.4
NGC 6752	18	62	336.8	-25.2	2190 \pm 289	4.263 \pm 0.862	539.0 \pm 50.3
Hydra 20a	20	62	261.4	37.6	1376 \pm 221	3.470 \pm 0.531	539.8 \pm 69.3
Hydra 20b	20	49	267.5	38.1	1211 \pm 184	3.054 \pm 0.619	478.5 \pm 37.1
Hydra 20c	20	64	273.5	38.5	1361 \pm 228	2.550 \pm 0.610	450.2 \pm 36.6
Hydra 21a	21	63	314.5	35.3	2200 \pm 227	5.409 \pm 0.673	539.0 \pm 63.2
Hydra 21b	21	50	309.5	38.3	2379 \pm 241	8.165 \pm 1.209	774.7 \pm 72.5
Hydra 21c	21	62	304.3	40.7	2179 \pm 210	7.063 \pm 1.152	709.7 \pm 103.3

$\delta < -40^\circ$. The averages listed in columns (7) and (8) were performed over the same $0.5^\circ \times 0.5^\circ$ pixels for which the average UV intensities were determined.

The data reduction, point source removal, and the treatment of foreground light sources for the FAUST images was described in detail by Sasseen et al. (1995). An additional discussion of the impact of the space shuttle environment on the astronomical observations and the removal of such effects is provided by Lampton et al. (1993) and Chakrabarti et al. (1993). With contributions due to direct starlight effectively removed (Cohen et al. 1994), the residual UV intensities listed in column (6) of Table 1 should therefore contain mainly a sum of DGL, residual airglow, and an essentially isotropic cosmic background.

Small, additional contributions to the diffuse emissions from the galaxy are likely in the form of H_2 fluorescence (Martin et al. 1990) and of line emission from C IV at 155.0nm, Si IV at 139.7nm and O [III] at 166.3nm (Martin & Bowyer 1990). Martin et al. (1990) detected about 75-150 units at low and intermediate latitudes for H_2 fluorescence, while Martin & Bowyer found < 20 units for the listed line emissions. These intensities are small compared to the variations in the airglow component, and lacking the facility to separate them spectroscopically in the FAUST experiment, we will include these emissions in the airglow component in subsequent sections and use DGL to refer only to dust-scattered radiation.

We confirm the presence of a strong DGL component in the data by plotting the observed average UV intensities for our 14 target fields against the corresponding HI column densities in Figure 1. The DGL component is expected to depend upon the column density of dust and upon the illumination conditions of this dust set by the galactic radiation field. The column density of dust is correlated with the HI column density (Bohlin et al. 1978). Hence, we expect a correlation between the DGL component and HI which Figure 1 indeed reveals.

We also note the interesting fact that the variation in the UV intensity in individual fields (Table 1) compared to the variation of the HI column densities for the same fields is larger on average (ratio = 3.62 ± 1.37 [photon units/ 10^{18} cm^{-2}]) than the same ratio (Fig.1) for the total data set (2.50 ± 0.37 [photon units/ 10^{18} cm^{-2}]). This is easily understood if one considers the difference in spatial resolution represented by the two data sets, $30' \times 30'$ pixels for the UV intensity measurements vs. the 2° FWHM width of the horn beam of the Bell Lab HI survey. We infer that there must be real intensity variations in the UV background radiation due to structure in the ISM too small to be resolved by the HI survey.

The positive intercept at $N(\text{HI}) = 0$ in Figure 1 suggests that the sum of residual airglow and extragalactic background is approximately 600 units. It is likely that this

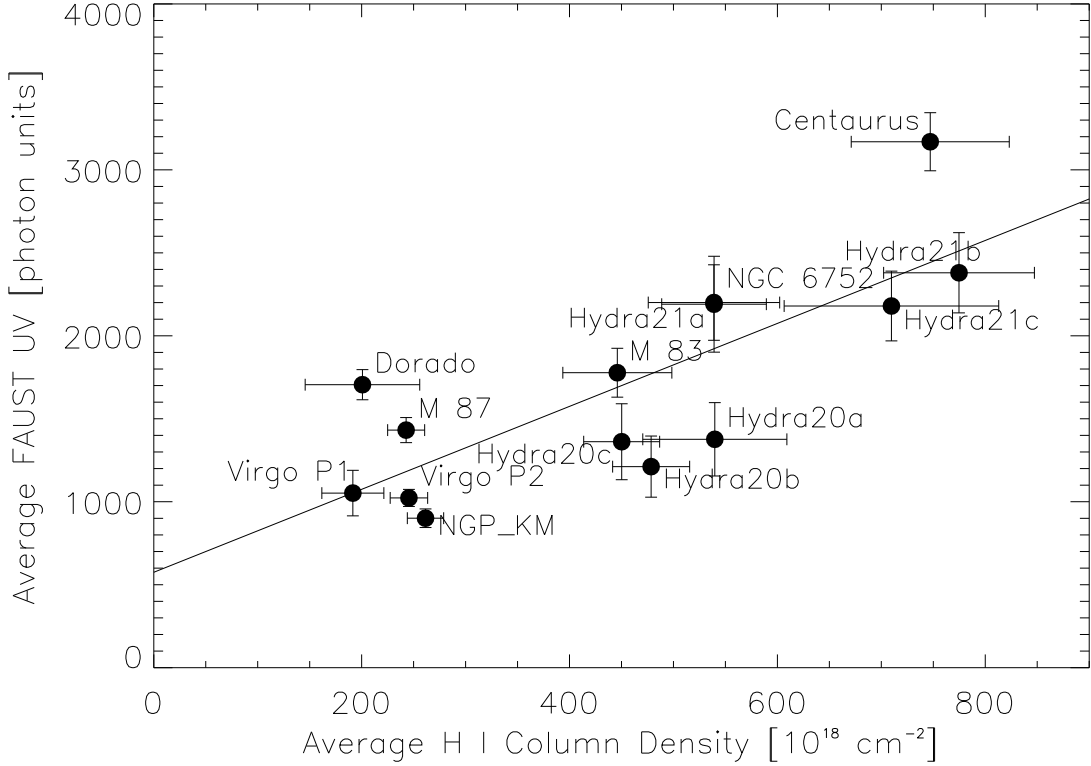


Fig. 1.— A plot of the average diffuse UV background intensity measured in 14 FAUST fields against the average HI column densities. Averages are performed over a $4^\circ \times 4^\circ$ area centered on the field coordinates. The error bars represent one standard deviation of the distribution of values about the respective averages.

is an underestimate because the coupling of a forward-throwing phase function with the concentration of galactic light sources near the galactic plane produces a higher scattered light intensity per unit dust column at lower latitudes, i.e., higher $N(\text{HI})$ values, compared to higher latitudes, or lower $N(\text{HI})$ values, thus steepening the slope of the correlation and lowering the corresponding intercept (WP 1994). We can test this by plotting the UV intensities against corresponding $100\mu\text{m}$ IRAS background intensities, as shown in Figure 2. The IRAS background is correlated both with the dust column density and the density of the interstellar radiation field responsible for heating the grains along the line of sight. The steepening of the correlation suspected in Figure 1 should therefore be reduced; a residual effect could still result from the decrease of radiation density with z -distance from the galactic plane.

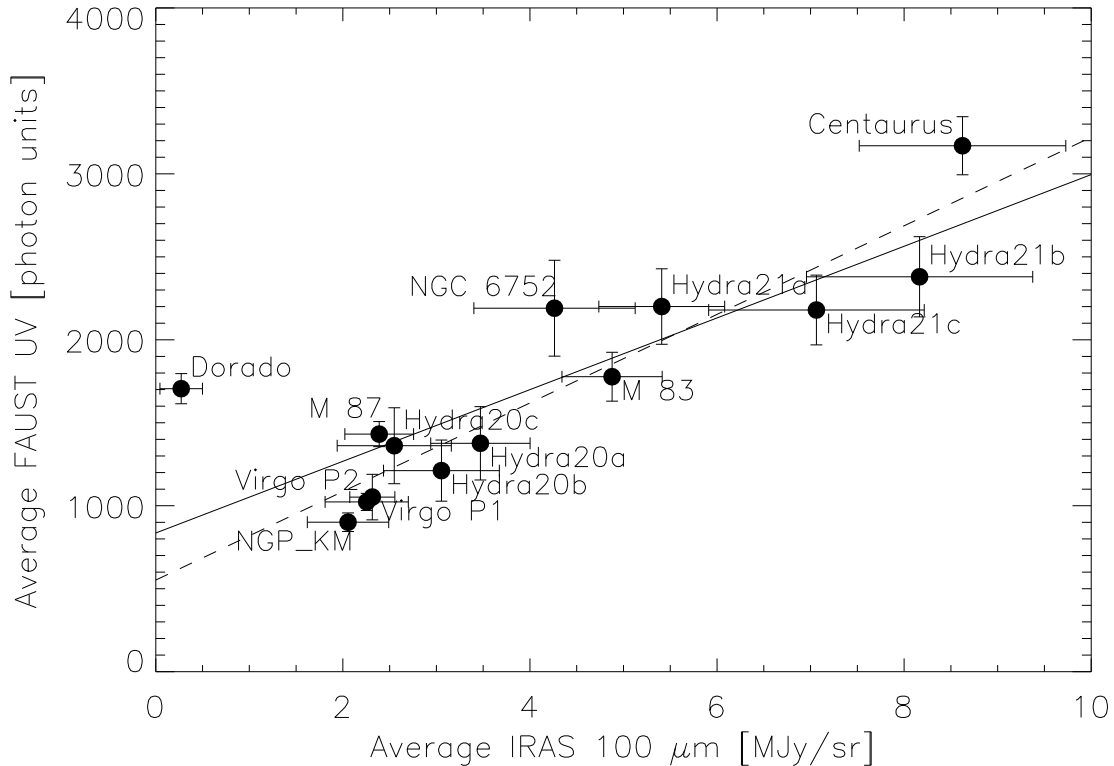


Fig. 2.— The same UV intensities as in Fig. 1 plotted against the diffuse Galactic IRAS $100\mu\text{m}$ background intensity. The solid line indicates the linear correlation involving all data points; the dashed line shows the linear correlation for the data with the Dorado measurement excluded.

In Figure 2, the intercept at zero IRAS intensity suggests a background of about 835 units, as suggested above. However, this is rendered somewhat uncertain by three factors: (1) the zero-point uncertainties (Boulanger & Péroult 1988) of the IRAS $100\mu\text{m}$ detector; (2) the likely presence of an as yet undetermined extragalactic background component in the $100\mu\text{m}$ intensity; and (3) the exceptional weight of the Dorado measurement on the slope of the correlation. Since the high UV intensity at Dorado is consistent with expectations from our model (see Figure 5), we suspect that the $100\mu\text{m}$ intensity of Dorado is in error. Eliminating Dorado from the correlation in Figure 2 (dashed line), we arrive at an intercept of 550 units, in essential agreement with the intercept in Figure 1. The closeness of the correlation between DGL and far-IR background in Fig. 2 is marginally better ($r = 0.93$, Dorado omitted) than the correlation between DGL and HI in Figure 1 ($r = 0.79$); this may be understood through the fact that both DGL and IRAS $100\mu\text{m}$ intensities depend

directly on the dust column density, while the DGL-HI correlation involves a possibly variable gas-to-dust ratio. We must attribute the real width in the DGL distribution for a given IRAS intensity as resulting from variations due to phase function effects in the far-ultraviolet, which would leave the IRAS background unaffected, and from deviations of the line-of-sight cloud spectrum from the average (see §3.3.4).

This initial examination of the FAUST data revealed that the measured diffuse background intensities consist of a constant component of at least 600 units and a DGL component which is correlated with other measures of the galactic dust column density and with the galactic radiation density. Provided the first component is, on average, the same for any random subset of the data, the latter component can be analyzed with an appropriate radiative transfer model.

3. The Radiative Transfer Model

3.1. General Requirements

A successful model for the DGL must have the following properties: (1) It must contain the actual observed illuminating radiation field, (2) the scattering medium should have cloud structure, and (3) multiple scattering must be included. These requirements become clear when one considers the following points.

One of the most important characteristics of the DGL at far-UV wavelengths is apparent from Figure 1: The DGL intensity for a given $N(\text{HI})$ varies by factors of two-to-three with direction in the sky after the approximately constant background has been subtracted. While part of this variation may be due to a spatially variable gas-to-dust ratio or to dust associated with HII or H_2 rather than HI, most of the observed variation is a result of the spatially, severely anisotropic, interstellar radiation field (Gondhalekar 1990; Henry et al. 1988). A first requirement of any suitable DGL model for the UV is therefore that it must employ the known distribution of the far-UV sources of radiation. A radiation field based on the expected UV fluxes from known hot stars listed in the SKYMAP star catalog (Gottlieb 1978) has recently been presented by Murthy & Henry (1995). Another useful source is the measured UV fluxes of some 58,000 stars detected by the TD-1 satellite (Gondhalekar 1990), which we have used for this work.

The interstellar medium responsible for the opacity of interstellar space is distributed in the form of structures commonly referred to as clouds. Clouds containing grains with single-scattering albedo $a < 1$ and exposed to an external radiation field will have an albedo less than the single-scattering albedo (van de Hulst 1987), and this difference in albedo will

become larger with increasing optical depth of a cloud and with increasing phase function asymmetry (Witt & Gordon 1996). In the far-UV the optical depth per cloud is typically three times that at visible wavelengths, and previous studies suggest an increase of the phase function asymmetry toward shorter wavelengths (Calzetti et al. 1995). Thus, a DGL model suitable for the analysis of far-UV data should incorporate a cloud structure for the scattering medium if it is to avoid a systematic underestimate of the far-UV albedo.

Van de Hulst and de Jong (1969) demonstrated that multiple scattering is an indispensable feature involved in the transfer of DGL. This applies even more to the UV because of the greater optical depths of the galactic dust layer. In the case of the present observations, which are restricted to intermediate and high galactic latitudes with $N(\text{HI}) \leq 8 \times 10^{20} \text{ cm}^{-2}$ (see Table 1), multiple scattering is marginally important. With corresponding UV optical depths of order 1.2 or less, the resultant albedo bias can be as high as 25% if the entire line-of-sight material is contained in a single cloud and a single grain albedo of 0.5 is assumed. We will, therefore, include multiple scattering in our model.

3.2. Model Design

The principle of the WP radiative transfer model follows the pioneering approach of Mattila (1971) by taking into account the discrete cloud structure of the interstellar medium. Mattila’s treatment was limited to directions in the galactic plane which placed his calculations into the limit of very large optical depths. This meant that the DGL intensity was determined mainly by the adopted incident radiation field which was derived from photometric measurements of the integrated sky brightness as a function of galactic latitude and longitude.

In the WP model, the approach was generalized to include all galactic latitudes. As a source for the (mostly small) optical depths at higher latitudes we adopted the Bell Laboratories HI Survey (Stark et al. 1992), supplemented by the Parkes HI survey (Cleary et al. 1979; Heiles & Cleary 1979). We used the conversion from HI column density to optical depth at the FAUST effective wavelength of 165nm as given by Sasseen & Deharveng (1996),

$$\tau_{165} = 0.144N_H[10^{20} \text{ cm}^{-2}], \quad (1)$$

which is based on the $N(\text{H}) - E(\text{B}-\text{V})$ relationship observed by Bohlin et al. (1978) and Diplás & Savage (1994), and the average galactic extinction curve of Savage & Mathis (1979).

3.2.1. Radiation Fields

In order to extend the radiative transfer model to directions with $|b| > 0^\circ$, we need to express the variation of the radiation field with z -distance from the plane. We start by constructing the radiation field in the galactic plane ($z = 0$) utilizing the fluxes of about 58,000 stars measured by TD-1 at $\lambda = 156.5\text{nm}$ (FWHM = 330\AA) which were kindly provided to us by J. Murthy. Maps of this radiation field may be found in the recent work of Murthy & Henry (1995) and in the Atlas of the Ultraviolet Sky by Henry et al. (1988).

The TD-1 catalog is thought to be complete down to fluxes of $1.0 \times 10^{-12} \text{ erg cm}^{-2} \text{ s}^{-1} \text{ \AA}^{-1}$ at 156nm. The contribution by stars fainter than this limit to the integrated stellar fluxes appears to be negligible at this wavelength, certainly much less than 10% of the total (Gondhalekar 1990). However, the DGL observed by TD-1 (Morgan et al. 1978) is part of the illuminating radiation field seen by each cloud and needs to be added to the integrated stellar flux. We therefore computed the expected DGL radiation field for a dust albedo $a = 0.5$ and a strongly forward directed phase function and added it to the integrated stellar fluxes. This increased the total background intensities by typically 25%.

For the purpose of our calculation, we represented this radiation field (at $z = 0$) as an 800-element, two-dimensional array, and expressed the average intensity in each array element in photon units. The spacing of the array elements and their sizes are non-uniform. At low galactic latitudes, and other directions where large gradients in the radiation field intensity occur, elements are spaced more closely, while at high galactic latitudes large elements are chosen.

The transformation of the central-plane radiation field into one seen by a cloud located at distance $z_C \neq 0$ from the galactic plane was approximated following a method described by Mattila (1980a,b). For the purpose of this transformation only, we assumed that the principal source of the $\lambda = 156.5\text{nm}$ radiation field is galactic OB stars whose volume emissivity is distributed in a plane-parallel disk with an exponential z -distribution characterized by a vertical scale height $\beta = 60 \text{ pc}$. We assume this because about 90% of the total integrated stellar radiation at 156nm arises near the galactic plane defined by $-45^\circ \leq b \leq 45^\circ$ (Gondhalekar 1990). Also, this assumption appears justified because the number of suspected subdwarfs in the TD-1 catalog, though greater than anticipated, was only of order 10^3 (Carnochan & Wilson 1983). The galactic distribution of these stars does not differ drastically from that of the overall stellar radiation field and their contribution to the radiation field was included in any case. By comparing the expected b -distribution of the integrated intensity seen by an observer at $z = z_C$ with the symmetric distribution seen at $z = 0$, we derived transformation factors as a function of z_C and b . This was done by dividing the skewed radiation field distribution at $z = z_C$ by the symmetric distribution at $z = 0$. To

obtain an actual radiation field applicable to $z = z_C$, we then multiplied the TD-1 radiation field with the appropriate b -dependent transformation factors. As a result, radiation fields at increasing $|z_C|$ exhibit a growing asymmetry in the radiation emanating from the two galactic hemispheres with $b > 0^\circ$ and $b < 0^\circ$, and the near-equatorial intensity peak shifts toward latitudes in the opposite hemisphere while maintaining the basic non-isotropy and longitudinal variability of the original TD-1 field. We constructed a total of 17 radiation fields, for values of $z_C = 0, \pm 25\text{pc}, \pm 50\text{pc}, \pm 75\text{pc}, \pm 100\text{pc}, \pm 150\text{pc}, \pm 200\text{pc}, \pm 250\text{pc},$ and $\pm 300\text{pc}$.

3.2.2. *Cloud Spectrum*

Interstellar clouds exist with a wide range of optical depths (e.g. Crovisier 1981). In order to reflect these conditions we adopted a cloud spectrum of three types of spherical clouds: uniform clouds of optical depth diameter (at 156.5nm) of 0.5, uniform clouds of optical depth diameter of 2.5, and centrally condensed clouds ($\rho \propto r^{-2}$ for $r/R \geq 0.05$; $\rho = \text{constant}$ for $r/R < 0.05$) of optical depth diameter of 10. The probability ratio of encountering such clouds along any line of sight was taken to be 12:3:1. Assuming arbitrary impact parameters for a penetrating line-of-sight, such a cloud spectrum provides, on average, a column density distribution very similar to that derived by Crovisier (1981) from the statistical properties of interstellar HI which were based on 21-cm line absorption surveys. The average optical depth per cloud for our adopted spectrum was found to be 0.593 by subjecting our spectrum of three clouds, in a frequency ratio of 12:3:1, to random penetration by a line of sight. The Crovisier study seemed to be particularly relevant in the current context: (1) its database consists mainly of observations out of the galactic plane, as is the case with the FAUST data; (2) our source for the column density of dust is the correlation between $E(B-V)$ and HI (Bohlin et al. 1978); (3) the range of total HI column densities covered by the Crovisier study coincides with the range encountered in the FAUST fields in this study.

The probability of encountering a cloud of any type at a distance z from the galactic plane was assumed to be given by an exponential distribution with a scale height of 110 pc, i.e. was assumed to be proportional to $\exp(-z/110 \text{ pc})$ (Crovisier 1981; Lockman 1984).

3.3. Model Operation

The computation of the expected DGL surface brightness in a given direction with our model involves several Monte Carlo processes: the multiple scattering radiative transfer within each cloud of our cloud spectrum, the determination of the number of clouds in a given direction, the determination of the type and location of the cloud along the line of sight, the determination of the individual surface brightness profile of each cloud along the line of sight, the determination of the penetration point of each cloud, the determination of the optical depth along the chosen line of sight through each cloud, and finally the integration of intensities of the clouds along the line of sight.

3.3.1. *The Radiative Transfer in Individual Clouds*

The transfer solution for a spherical cloud of given optical depth diameter, dust scattering parameters given by albedo a and phase function asymmetry g , and density profile was found with the method outlined in Witt & Stephens (1974) and in FitzGerald et al. (1976). The method traces the transfer of individual photons in reverse and produces weight matrices which express the probability that photons hitting the cloud from any direction will exit the cloud at a given projected radius in the direction of the observer. For the non-isotropic scattering phase function, the Henyey-Greenstein (1941) function was chosen. Our approach has the advantage that the radiative transfer through individual clouds needs to be done only once for a given set of parameters. The specific surface brightness profile exhibited by a cloud at a given z_C can be obtained by multiplying the cloud's probability matrix with the appropriate radiation field matrix corresponding to the value of z_C .

3.3.2. *The Number, Type, and Location of Clouds along the Line of Sight*

The average number of clouds along a given line of sight with total column density $N(\text{HI})$ is found by dividing the corresponding optical depth derived from Eq. (1) by the average optical depth per cloud $\langle \tau_C \rangle = 0.593$ (§3.2.2). For a typical line of sight in the galactic plane ($A_V = 1.9$ mag/kpc; Spitzer 1978), with an average ratio of $N(\text{HI})/E(\text{B-V}) = 4.8 \times 10^{21}$ atom cm^{-2} mag $^{-1}$ (Bohlin et al. 1978), we find 7.1 clouds/kpc, in close agreement with estimates discussed by Spitzer (1978). For typical high- $|b|$ lines of sight, we generally find 2, 1, or no clouds.

The actual number of clouds, n , for a given Monte Carlo simulation is then selected

by a Monte Carlo process from a Poisson distribution whose average is the average number of clouds just determined. The types of clouds (optical thickness diameter, density distribution) are found by random-number choices from within our cloud spectrum based upon their relative frequencies. The z-distances of these clouds are then derived from yet another series of Monte Carlo processes applied to the assumed exponential distribution of cloud distances from the Galactic plane. This sampling of cloud distribution by number, types, and location along the line of sight was performed 300 times for each of the approximately 60 pixel positions within each FAUST field for a total of 1.8×10^4 integrations per field. Thus, the statistical properties of the interstellar medium are interwoven into the prediction of the DGL intensity. We therefore predict an actual distribution of expected DGL intensities for each pixel, whose FWHM provides a measure of the DGL uncertainty resulting from possible deviations from average conditions. Examples of such distributions are shown in Figure 3 and will be discussed below in §3.3.4.

3.3.3. *Surface Brightness Profiles and Total DGL Intensities*

The probability weight matrix of each of the randomly selected and positioned clouds (§3.3.2) must be multiplied by the appropriate radiation field in order to predict their radial surface brightness profiles. The most abundant variety of clouds, the optically thin ones, exhibit a brightness profile with a maximum at the projected center; the moderately optically thick clouds present a fairly flat surface brightness profile with limb darkening, while the highly optically thick clouds display a dark central region surrounded by a bright rim (Witt & Stephens 1974). The surface brightness value added by each cloud along the line of sight is determined by the selection of a random penetration point on the geometric cross section of a cloud. In order to correct the surface brightness of still more distant clouds seen in this direction, we also determine the optical depth through the entire cloud at the penetration point. If the intensities of the clouds along a given direction are denoted by I_1, I_2, I_3, \dots , the total integrated intensity for this line of sight (Mattila 1971) is

$$I_{DGL} = I_1 + I_2 e^{-\tau_1} + I_3 e^{-(\tau_1 + \tau_2)} + \dots \quad (2)$$

3.3.4. *Dependence of Results on Model Parameters*

In its attempt to represent the DGL radiative transfer in as realistic a manner as possible, the model described above involves numerous parameters. While most of these, such as the radiation field distribution and the optical depth distribution, are well constrained by available observations and may therefore be considered fixed, it is the nature

of the adopted cloud spectrum that affects the model predictions most profoundly. As indicated in §3.1, the greater the optical thickness of an individual cloud, the lower its resultant effective albedo for a given radiation field and single grain albedo. In addition, in directions with low column densities, a cloud spectrum incorporating clouds of higher optical depth naturally leads to instances of "holes", i.e. directions with no clouds and thus, zero DGL intensity, because the beam-averaged optical depth must still be that constrained by the HI column density. If, on the other hand, the cloud spectrum consists entirely of very-low- τ clouds, there will always be numerous clouds along lines of sight with small overall column density, assuring a more uniform sky coverage with more efficiently scattering clouds.

We illustrate these effects in Figure 3 by showing the results of 100 samplings with 300 photons each along a single direction ($\ell = 315^\circ, b = +35^\circ, N(\text{HI}) = 5.15 \times 10^{20} \text{cm}^{-2}$) for three different cloud spectra. The first consists of optically thin clouds of type 1 only, with an optical depth diameter of 0.5 at 156.5nm wavelength. The average optical depth for cloud penetration is 0.33. The predicted DGL intensity is 1871 ± 59 units. The second is our adopted case of a cloud spectrum with ratios 12:3:1 divided among clouds of type 1, 2, and 3, respectively. The average optical depth per cloud is now 0.59 and the predicted DGL intensity is 1329 ± 52 units, some 30% lower than case 1. The third case displayed is for a cloud spectrum 1:1:1, which now emphasizes optically thick clouds. The average optical depth per cloud is 0.83 and the predicted DGL, as expected, is still lower at 1101 ± 52 units. All calculations assumed the same scattering characteristics, namely $a = 0.45$ and $g = 0.675$.

For the analysis of the FAUST data we have adopted a cloud spectrum which is dominated by low- τ diffuse clouds, but also contains a small number of clouds of greater optical thickness in a ratio of 12:3:1 in terms of their average relative frequency along a given line of sight. This spectrum reflects the demonstrated presence of numerous small molecular clouds at high galactic latitudes (Magnani et al. 1986; Magnani et al. 1996; Stark 1995; see Magnani 1994 for a recent review). Our adopted spectrum is also consistent with the observed distribution of HI column densities based on the 21-cm line absorption survey by Crovisier (1981). It should be clear from Fig. 3 that the albedo derived from the FAUST data using our adopted cloud spectrum will be higher by about 30% than it would be, had we assumed low- τ clouds entirely. The dependence of the intensity of the predicted DGL upon the chosen cloud spectrum must also be kept in mind when we compare predicted DGL intensities with those actually observed (see Fig. 6).

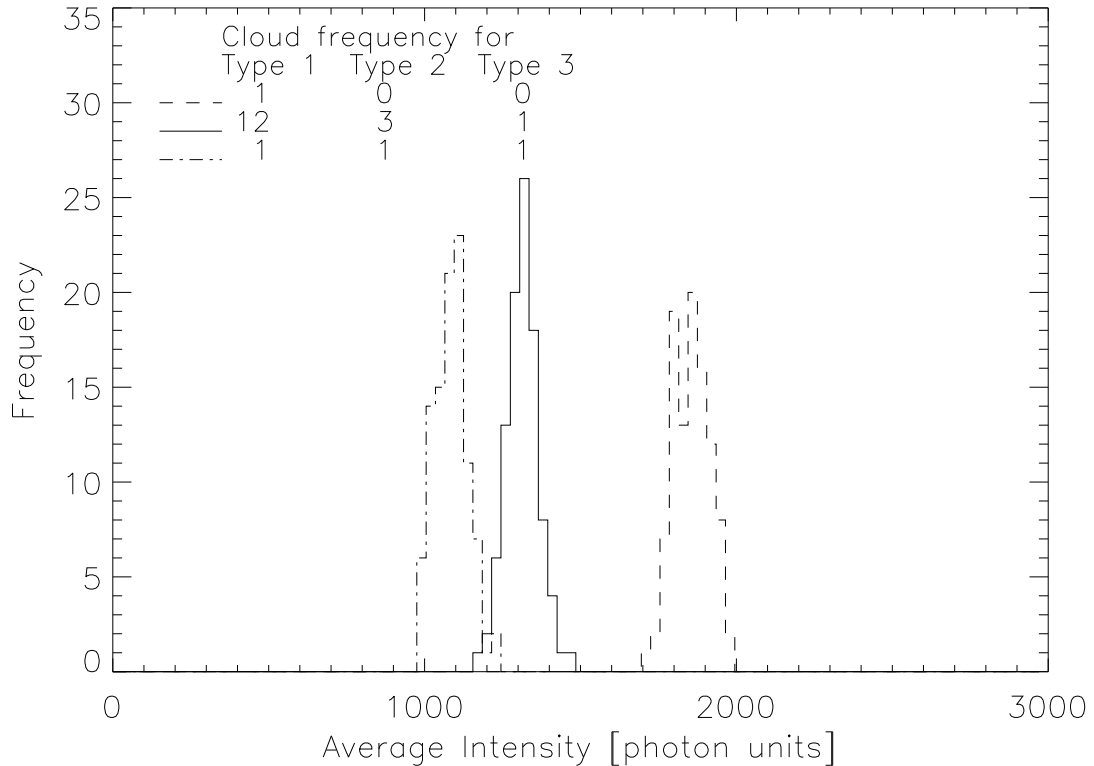


Fig. 3.— Model prediction of the intensity of UV DGL plus UV background derived from 100 samplings with 300 photons each for three different cloud spectra. All calculations are for the identical direction ($\ell = 315^\circ$, $b = +35^\circ$) and for identical grain properties ($a = 0.45$, $g = 0.675$). The hydrogen column density is $N(\text{HI}) = 5.15 \times 10^{20} \text{cm}^{-2}$.

4. Derivation of Scattering Properties

Our aim in this section is two-fold: (1) We want to separate the galactic component of the diffuse UV intensities measured by FAUST (Table 1) from the non-galactic components. Contributions to the latter are terrestrial airglow and extragalactic background radiation. (2) We want to analyze the galactic component using the DGL model described in the previous section. The aim is to derive the average dust albedo a and the average phase function asymmetry parameter g which characterize the galactic dust in the diffuse ISM at intermediate and high galactic latitudes. Toward this end we calculated the expected average UV intensity for each of the 14 FAUST fields, each based on approximately 1.8×10^4 integrations, for a wide grid of closely spaced values of a and g .

4.1. The Fitting Criteria

Which set of scattering parameters for dust grains will lead to the best representation of our data? To decide this question, we assumed the following. (a) All FAUST lines of sight contain dust with identical average properties. Since for our observations $|b| > 21^\circ$, most of the clouds studied are well outside the galactic plane and are representative of the low-density diffuse interstellar medium. (b) The measured surface brightness of each FAUST field contains an unknown component with a surface brightness ≥ 0 units due to residual airglow and a component of extragalactic origin. We assume the latter to have an intensity of 300 units (WP 1994) outside the Galaxy. This component is assumed to be isotropic but to be attenuated for each line of sight by the galactic dust column derived from the $N(\text{HI})$ values. We included this extragalactic component both into the illuminating radiation field (essentially negligible) and into the predicted intensity for each FAUST field. (c) On average, the FAUST fields at lower galactic latitudes are subject to the same airglow contamination as the FAUST fields at higher galactic latitudes. This does not require that each field have an identical airglow component, only that any random group of six or seven fields have similar airglow averages. Thus, the galactic latitude dependence seen in our measured intensities is due entirely to DGL and the extinction-modulated extragalactic background with the former generally increasing with decreasing latitude and the latter decreasing with the increasing extinction at lower latitudes. Given these assumptions, the best-fit model must satisfy these requirements:

1. Slope Criterion: The model predictions of the DGL values for the FAUST fields, including the partially attenuated extragalactic radiation, must exhibit the same slopes as the observations when plotted against the corresponding values of $N(\text{HI})$, $\text{cosec}|b|$, and the IRAS $100\mu\text{m}$ intensities for the FAUST fields.
2. Positive Airglow Criterion: The average predicted intensities of DGL and extragalactic light for individual FAUST fields should in no case fall above the measured intensities since this would imply negative airglow.
3. Equal Airglow Criterion: A considerable range of dust scattering parameters (a, g) will be able to satisfy the first two criteria. However, for most sets of values of (a, g) , the value of the positive airglow derived from application of criteria (1) and (2) is different when observations and model predictions are plotted against $N(\text{HI})$ and when plotted against $\text{cosec}|b|$. The equal airglow criterion demands that the value of the airglow deduced from the comparison of intercepts is the same when observations and model predictions are plotted against $N(\text{HI})$ and $\text{cosec}|b|$ and evaluated at $N(\text{HI}) = 0$ and $\text{cosec}|b| = 0$.

A much more limited set of values (a, g) will satisfy this third criterion in addition to satisfying the first two. We do not include the intercept in the plot against the IRAS $100\mu\text{m}$ diffuse intensity in this criterion because calibration uncertainties in the zero point of the IRAS intensity scale and the presence of some extragalactic component in the IRAS data would render the outcome uncertain.

4.2. Models

In Figure 4, we show all combinations of a and g for which complete models were calculated. Different symbols indicate the slope found when predicted intensities are plotted

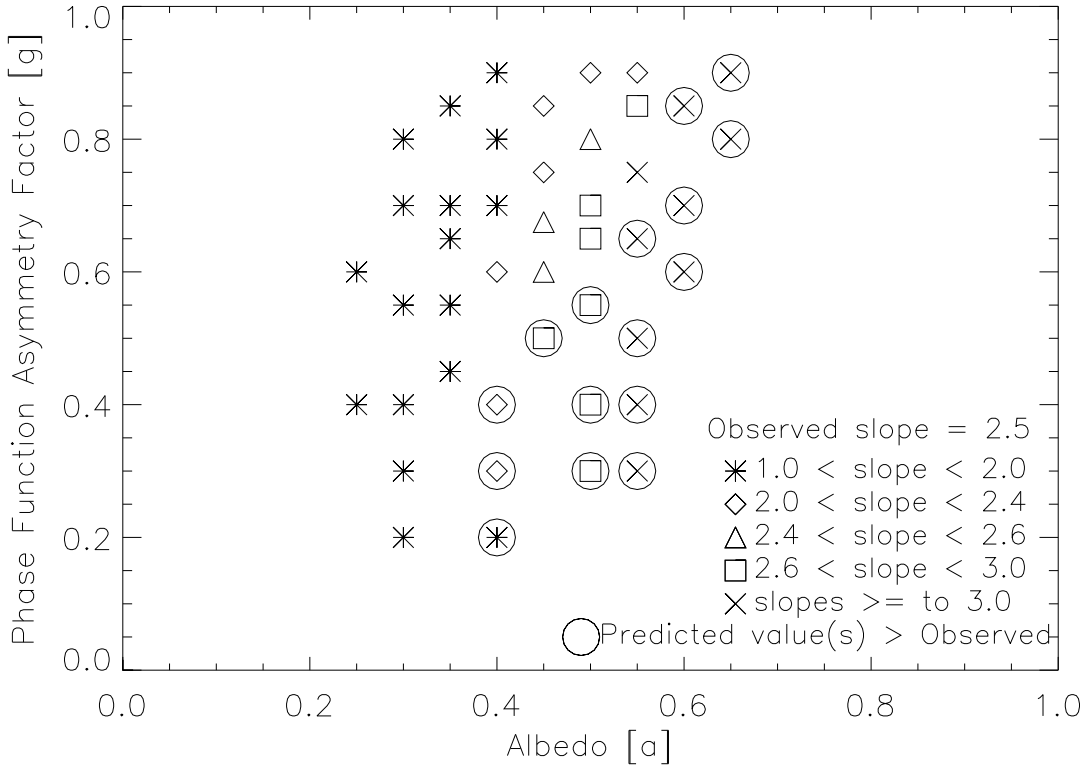


Fig. 4.— Complete models were calculated for the grain scattering properties indicated by the symbol locations in the (a, g) plane. Different symbols indicate the slopes in graphs of the predicted UV intensities vs. $N(\text{HI})$. The encircled symbols correspond to models which predict intensities higher than observed.

against the $N(\text{HI})$ values for the corresponding FAUST fields. The observed slope (see Fig.

1) is 2.5 [photon units/ 10^{18}cm^{-2}]. It is clear from Fig. 4 that the fitting criterion (1) is met within a very narrow range of a -values ($0.4 < a < 0.5$) but for a large range of g -values. The positive airglow criterion eliminates all models identified by encircled symbols, as well as all those with still larger a -values which were left uncomputed.

As an example, a model with $a = 0.45$ and $g = 0.675$ is shown in Fig. 5 in comparison with the FAUST data plotted against the $N(\text{HI})$ values of the corresponding FAUST fields. The model points, denoted by open circles with vertical error bars, follow the observed

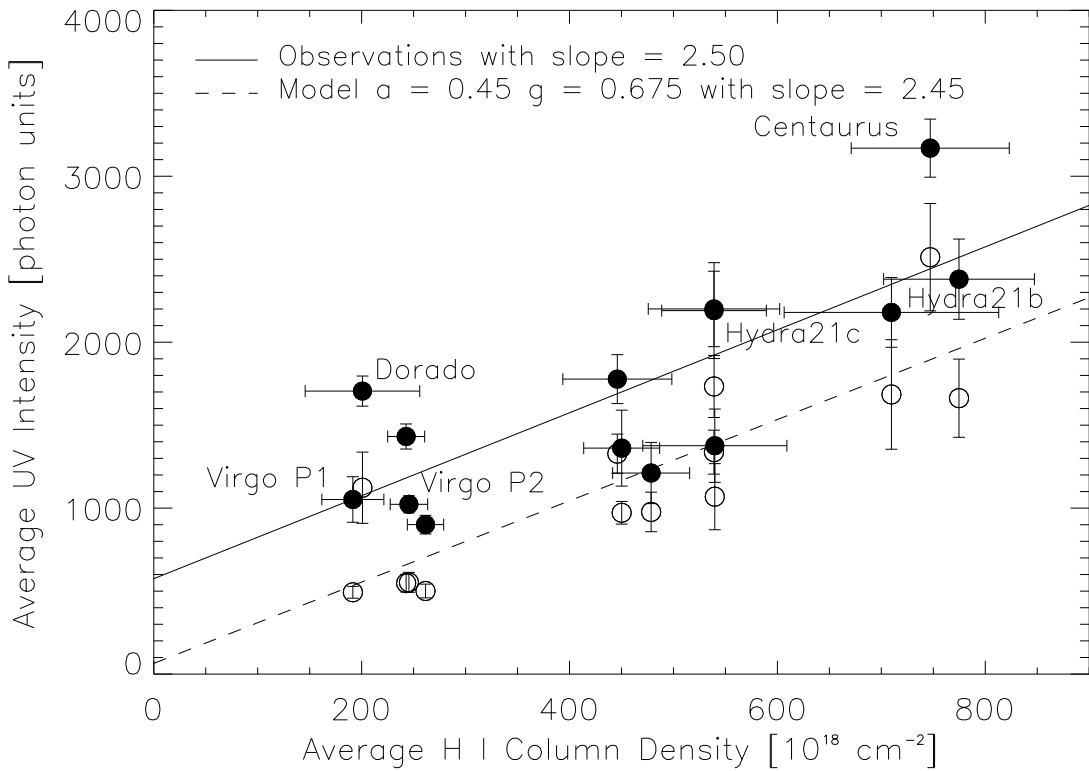


Fig. 5.— Model predictions (open circles) are plotted together with corresponding observations against average $N(\text{HI})$ values for FAUST fields. The vertical model error bars denote one standard deviation in the distribution of predicted intensities for a $4^\circ \times 4^\circ$ field.

intensities closely, except they are displaced by a constant vertical offset attributed to the airglow component. For example, the model successfully reproduces the significant differences in intensity observed for groups of FAUST fields for which the HI column density is almost constant. Specific cases are the groups consisting of Hydra 21c, Centaurus and Hydra 21b, and Virgo P1, Dorado, and Virgo P2. This gives us confidence both in the

model’s predictive power and in our assumption that the residual airglow contribution is roughly constant. Note that the positive airglow criterion (2) is also met in the model shown in Fig. 5.

To further illustrate the close match between the model predictions with the individual observations, we added an average airglow intensity of 530 units to the model values and overplotted these on the observations in Figure 6. In almost all cases, the observations are

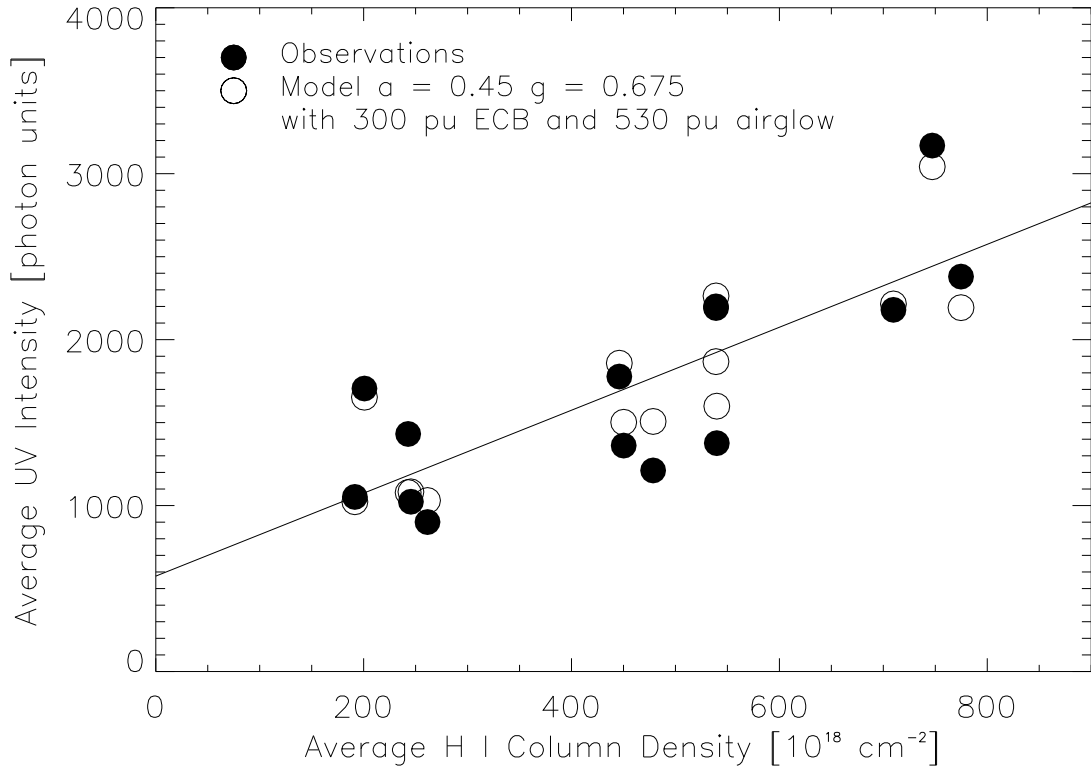


Fig. 6.— The same data and model predictions as in Figure 5, except that a constant airglow intensity of 530 units has been added to the model points. Error bars have been omitted for clarity; they would be identical to those shown in Figure 5. Note that the observed points for NGC 6752 and Hydra 21a essentially coincide. The corresponding model points are those immediately above and below the observed points.

reproduced within better than one standard deviation.

4.3. The Equal Airglow Criterion Applied

Thus far we have found combinations of a and g which reproduce the slope of the observed data in Figure 5.

As mentioned, we interpret the vertical offset between the least-squares slopes fitted to the observed points and the predicted points in Fig. 5 as resulting from airglow. The airglow intensity derived from Fig. 5 is about 530 units, on average. When the same data and predictions are plotted against $\text{cosec}|b|$ of the positions of the FAUST fields, we arrive at Fig. 7. Again, the observed and the model slopes are nearly identical and the vertical

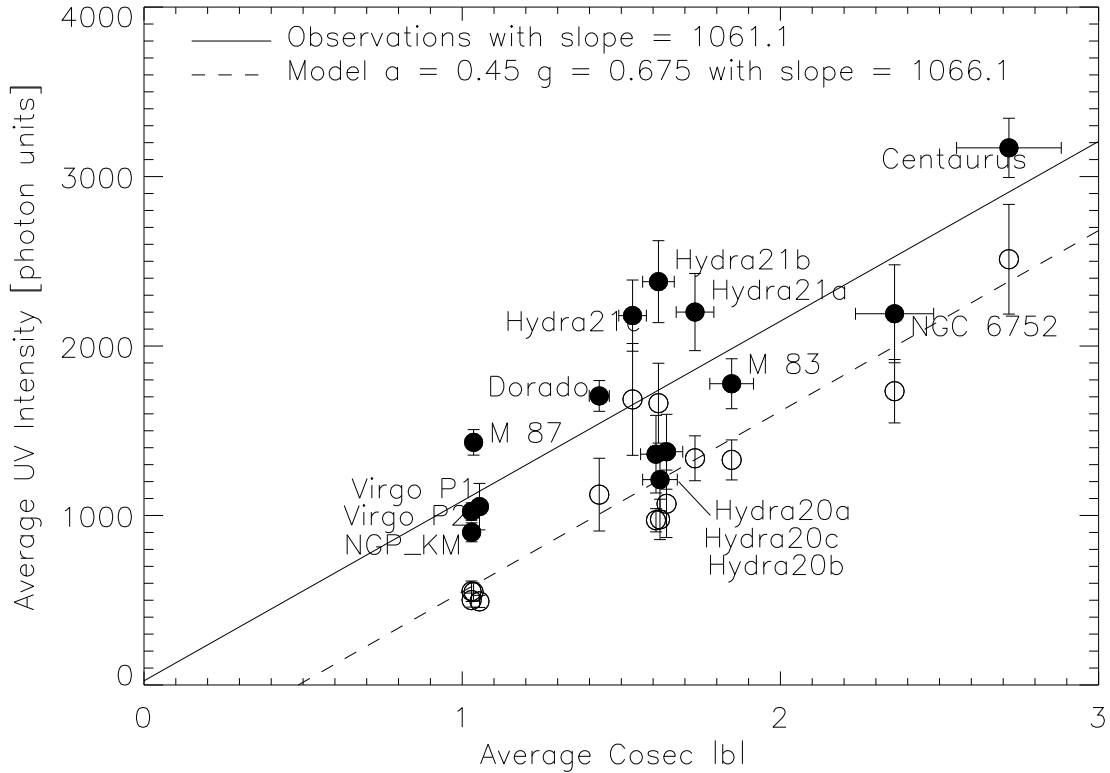


Fig. 7.— The same data and models as in Figure 5 plotted against $\text{cosec}|b|$ of the FAUST fields. The “best fit” solution shown here requires that the vertical offset between observed slope and model slope be the same as in Fig. 5.

offset between the two slopes is approximately 530 units, i.e., the inferred airglow intensity is the same as derived from Fig. 5. If the g -values of the models are increased beyond 0.675, the $\text{cosec}|b|$ plot yields higher airglow values than the N(HI) plot as well as divergent slope

values; if g is reduced below 0.675, the reverse occurs. This is shown quantitatively in Fig. 8 where lines of constant airglow as derived from the two types of plots are shown in the relevant area of the (a, g) plane. Allowable values for a and g must be located in the part of the plane where the two comparisons yield the same airglow values.

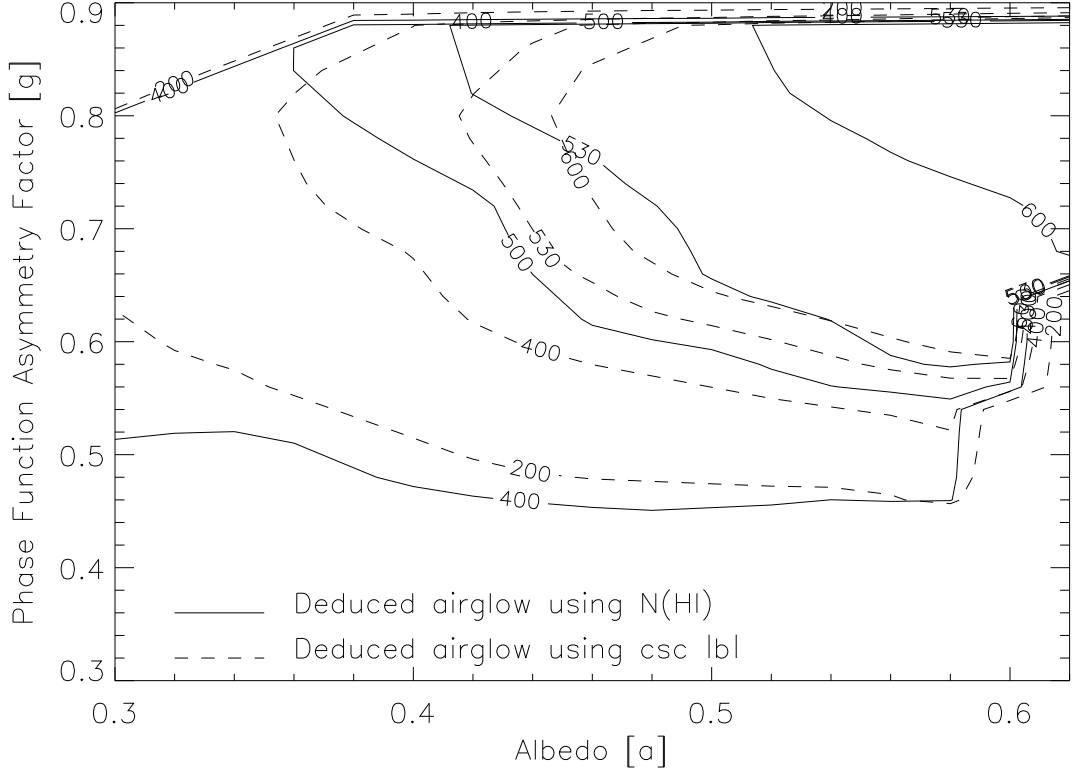


Fig. 8.— Contours of constant airglow deduced from comparing models and observations when plotted against $N(\text{HI})$ and against $\text{cosec}|b|$. This graph suggests an average airglow near 510 photon units as being associated with the “best fit” solution.

The straight forward application of the three fitting criteria constrains the best solution to a narrow region surrounding the point $a = 0.45$ and $g = 0.675$ in the (a, g) plane. Using this solution, we have derived the likely airglow intensities for our 14 FAUST fields and have listed them in Table 2.

Table 2. Deduced Airglow Values¹

FAUST Field	Deduced Airglow (Photon units)
Dorado	582 ± 233
NGPKM	400 ± 70
M 87	883 ± 93
Virgo P2	470 ± 79
Virgo P1	559 ± 142
Centaurus	657 ± 368
M 83	449 ± 368
NGC 6752	457 ± 344
Hydra 20a	307 ± 298
Hydra 20b	307 ± 220
Hydra 20c	390 ± 239
Hydra 21a	863 ± 263
Hydra 21b	717 ± 338
Hydra 21c	494 ± 391

¹Based on the assumption that the extragalactic isotropic background before galactic extinction is 300 photon units.

4.4. Uncertainties

It was shown in Fig. 4 that the albedo value of the "best fit" solution is sensitively dependent upon the slope of the measured FAUST diffuse intensity plotted against $N(\text{HI})$. Because of the close correlation between $N(\text{HI})$ and $\text{cosec}|b|$ and between $N(\text{HI})$ and the IRAS $100\mu\text{m}$ diffuse galactic background (Boulanger & Pérault 1988; Boulanger et al. 1996), the same would be the case, if plots are made against either of these two other quantities.

There are two major sources of uncertainty in these observed slopes: (1) The residual airglow is variable with time and direction, and thus, a randomly variable component is added to the true DGL values. The values in Table 2 are representative of the range of variability to be expected for the airglow component. Only if our DGL model were perfectly accurate would Table 2 give the actual airglow values, and we do not assume this. The presence of a random airglow component having the same distribution as Table 2 among our data renders the slope of the linear regression in the plot against $N(\text{HI})$ uncertain by ± 0.34 [photon units/ 10^{18}cm^{-2}]. (2) The absolute calibration of the FAUST instrument is uncertain by about 15% (Bowyer et al. 1993). While this does not affect the uncertainty of the linear regression, it affects each data point by the same percentage, and thus both the intercept and the slope are uncertain. We find the impact of the systematic calibration uncertainty upon the slope to be ± 0.37 [photon units/ 10^{18}cm^{-2}]. Adding these uncertainties in quadrature, we find for the observed slope 2.5 ± 0.5 [photon units/ 10^{18}cm^{-2}].

An additional uncertainty arises from the fact that two independent model calculations with identical parameters but different seeds for the random number generator produce model slopes which typically vary by ± 0.10 [photon units/ 10^{18}cm^{-2}], which must be added to the uncertainty above when observations and models are compared.

4.5. Scattering Properties

We again plot in Fig. 9 the (a, g) plane as in Fig. 4 in which the region of possible (a, g) values is now delineated by the application of the three fitting criteria and the uncertainties in the slope discussed above. The outer boundary is set by the slope uncertainty in the plot of FAUST intensities against $N(\text{HI})$. The cross-hatched area is considered unlikely for possible solutions since the model, with no airglow, overpredicts the observed intensity. The equal airglow criterion and the slope criterion lead to a most probable value for the albedo, $a = 0.45 \pm 0.05$, and for the phase function asymmetry, $g = 0.68 \pm 0.10$.

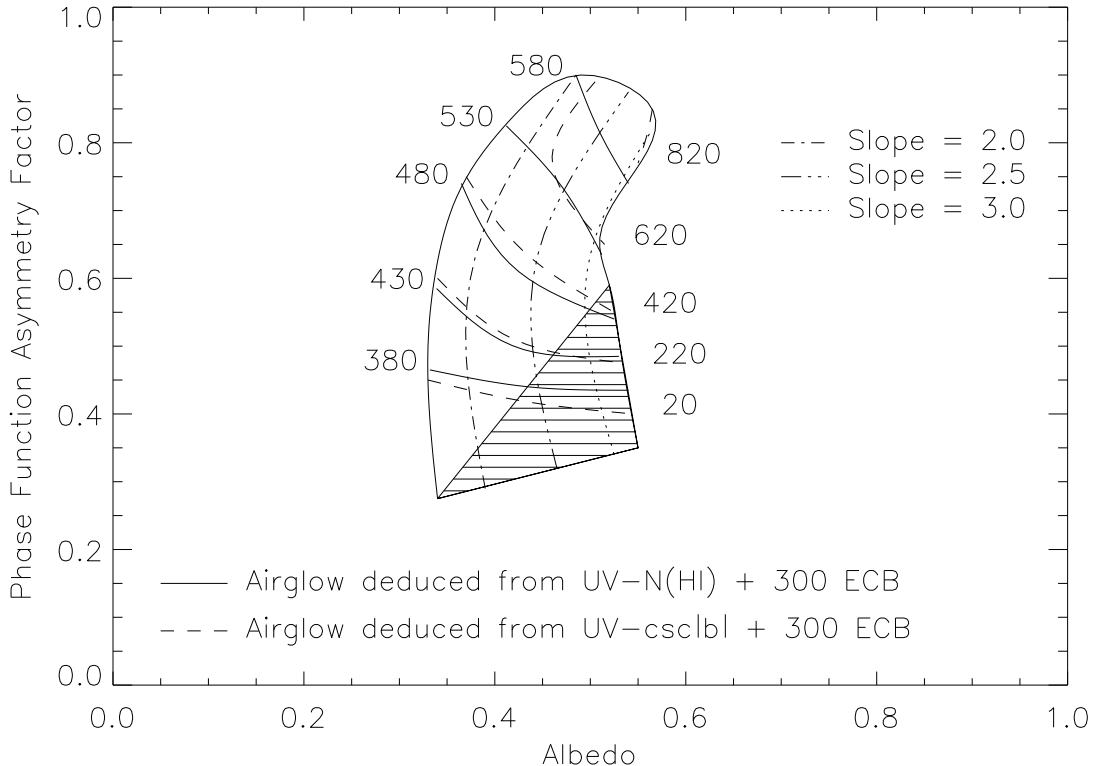


Fig. 9.— The derived scattering properties in the (a, g) plane as constrained by the three fitting criteria (§4.1). The slopes referred to are those of the predicted UV-DGL-N(HI) relationships.

5. Discussion

5.1. Scattering Properties

Ultimately, we would like to know whether the population of dust grains is different in different astrophysical environments within the Galaxy. Standard dust grain models are based mainly on the observation of the average galactic extinction curve (Savage & Mathis 1979) and observed depletions of heavy elements from the gas phase (Sofia et al. 1994; Snow & Witt 1995, 1996), and are therefore representing mostly the diffuse interstellar medium near the Galactic plane. However, differences in extinction characteristics between different lines of sight (Witt et al. 1984; Fitzpatrick & Massa 1990; Mathis & Cardelli 1992; Jenniskens & Greenberg 1993) as well as differences in depletion patterns (Sembach & Savage 1996) are well documented, and these are reflected in differences in the size

distributions of grains derived for different environments (e.g. Kim et al. 1994).

Scattering characteristics, like extinction properties, are also dependent on grain composition and size. There is little reason to suspect that dust grains in different environments, e.g. reflection nebulae, HII regions, or the low-density diffuse ISM, are similar with respect to their scattering properties. This is especially so in light of the considerable observational evidence that the extinction properties of the dust exhibit substantial variations in the UV, both in magnitude and in wavelength dependence.

In Table 3 we have compiled a number of values of (a, g) which have been derived recently from the observation and analysis of scattered UV light in reflection nebulae and star forming regions, all regions characterized by densities in the range $10^2 \text{ cm}^{-3} < n(\text{H}) \lesssim 10^4 \text{ cm}^{-3}$. The denser reflection nebulae appear to share albedo values in excess of 0.6 in the 130-170nm spectral range, while the present study yields a value definitely lower than that. This difference is most easily understood if we assume that the average grain size is larger in reflection nebulae, or, what would amount to the same, that the number of very small grains (size $\ll \lambda$) is reduced compared to the number of larger (size $\sim \lambda$) grains. This is indeed supported by the fact that in reflection nebulae $R_V = A_V/E(\text{B-V})$ is usually found to be larger than the "normal" galactic value for the diffuse ISM of $R_V = 3.1$, which is true also for the regions compared in Table 3. In addition, most of the dust observed in this study is seen at relatively high galactic latitudes, placing it potentially at large z -distances. With our assumed z -distribution, 50% of the dust is located at $|z| > 75 \text{ pc}$. Sembach and Savage (1996) have shown that dust grains in such environments are subject to erosive processes which return a portion of their solid substance to the gas phase. Kim and Martin (1996) have shown that size distributions of interstellar grains characterized by $R_V > 3.1$ have higher albedos than the standard $R_V = 3.1$ grains throughout the entire near-IR to UV spectral range. There are still discrepancies, however, between the observationally derived albedo values for reflection nebulae and the values predicted by Kim & Martin. This may simply reflect the fact that their assumed graphite/silicate composition for the grains does not correspond entirely to reality. Nevertheless, we have for the first time a relatively clear indication that the dust albedo in the UV in the diffuse ISM of the Galaxy is lower than the albedo in denser regions, about 0.45 vs. 0.65, and that this difference is related to the typical grain sizes found in these environments, with smaller grains in the diffuse ISM yielding a lower albedo.

Additional support for these conclusions is found in the observations and analysis of scattered far-UV radiation seen at high galactic latitudes by Onaka and Kodaira (1991). While more limited in spatial coverage, their data set allowed them to conclude $a \geq 0.32$ and $g \geq 0.5$, in agreement with our results. The suggestion of smaller dust grains, on

average, at higher $|z|$ - distances also finds support in the finding by Kiszczurno & Lequeux (1987) of a general steepening of the far-UV extinction curve with increasing $|z|$ -distance from the galactic plane. This characteristic is attributed to a systematic shift toward smaller grain sizes by these authors.

When comparing the phase function asymmetry values in Table 3, no clear difference can be established, and, in fact, may not exist. Within existing uncertainties, we conclude that the phase function asymmetry of scattering by dust in the diffuse ISM and in dense nebulae is identical. The phase function asymmetry is determined solely by those grains which contribute to the scattering. If, for example, the diffuse ISM contains a separate population of very small grains ($\ll \lambda$) which would provide absorption, the albedo would be lowered while the phase function would still entirely be determined by the larger scattering grains and would remain unchanged. In addition, a very small change in g represents a significant change in the phase function when $g \approx 0.7$, and as long as any determination of g is uncertain to ± 0.1 , any real differences equal to small Δg 's will not likely be detectable. The only situation which allows more precise differences in g to be derived is the determination of relative g -values as a function of wavelength in a given object (e.g. Calzetti et al. 1995).

5.2. The DGL-N(HI) Correlation

The positive correlation between the far-UV background intensity and the column density of neutral hydrogen is generally viewed as evidence for the Galactic origin of a major part of the UV background. (Lequeux 1990; Bowyer 1991). However, a number of separate investigations (Bowyer 1991, Table 1) have produced a wide range of values for the slope of the DGL-N(HI) correlation, often mutually exclusive. Bowyer (1991) tabulates values ranging from 0.3 to 1.8 [photon units/ 10^{18} HI cm^{-2}] from eleven different studies. To this, we now add our present result of 2.5 ± 0.5 [photon units/ 10^{18} HI cm^{-2}], larger than any found previously.

The significance of these apparent discrepancies is easily understood. The scattered light intensity per [10^{18} HI cm^{-2}] is determined by the scattering cross section per H-atom, the incident radiation field, and the phase function asymmetry g . A relatively large value of g , as we have deduced in this investigation, provides a strong coupling between the anisotropy of the illuminating radiation field and the anisotropy of the scattered radiation field. The FAUST observations were conducted in a region of the UV sky where the gradient in illuminating intensity between near-equatorial galactic latitudes and polar latitudes is one of the strongest in the entire sky. The fact that this strong gradient is indeed reflected

in a larger value for the slope in the DGL-N(HI) correlation is by itself an independent indication that the scattering phase function must be relatively large. Correlations between measured UV background intensities with N(HI) are therefore comparable only, if the data have been obtained from identical regions of the sky.

We can demonstrate that our value for the slope of the DGL-N(HI) correlation is well within the range expected for different regions of the sky with the following experiment. For this test, we adopted scattering properties $a = 0.45$, $g = 0.6$ and the average N(HI) values of the FAUST fields. We predicted the observable DGL, including 300 units of extragalactic background, for the actual FAUST fields and found a slope for the DGL-N(HI) correlation of 2.58 [photon units/ 10^{18} HI cm^{-2}] (Fig. 10). Retaining the galactic latitudes of the FAUST

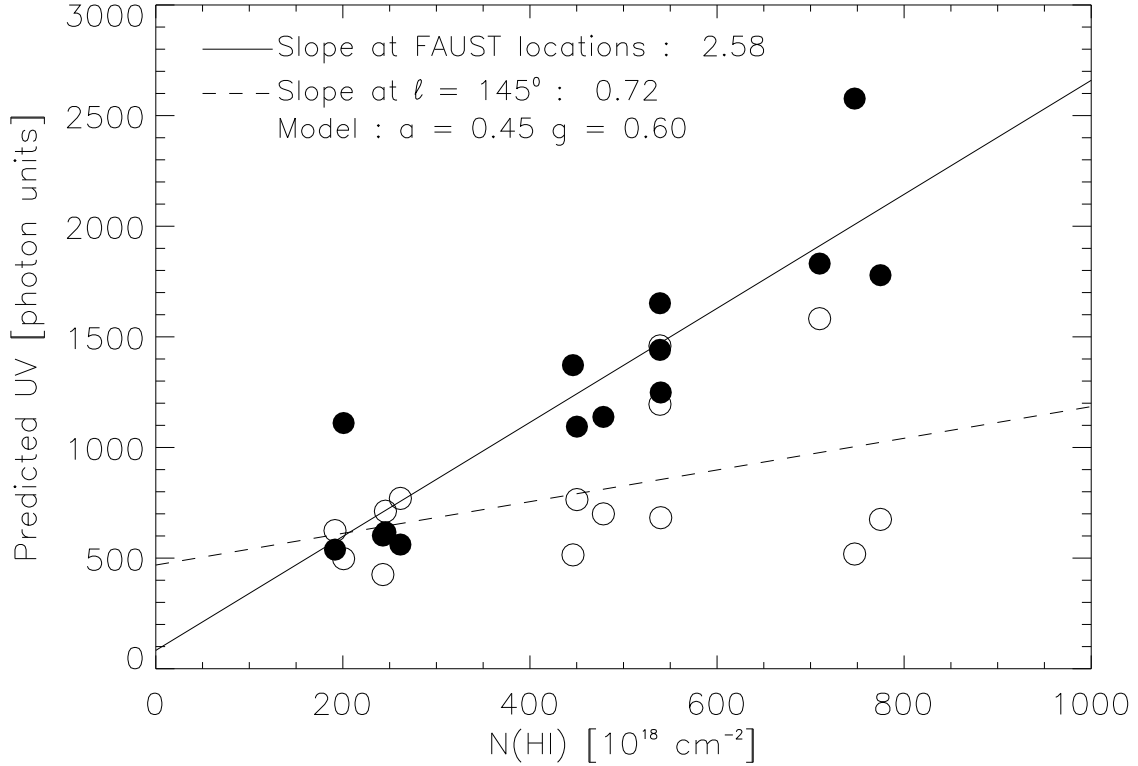


Fig. 10.— Predicted correlation between UV DGL and N(HI) for two different Galactic regions, assuming $a = 0.45$, $g = 0.60$; the actual positions of the FAUST fields (filled circles; slope = 2.58 [photon units/ 10^{18}cm^{-2}]) and hypothetical positions with the Galactic latitudes and N(HI) values identical to the FAUST positions, but moved to $\ell = 145^\circ$ (open circles; slope = 0.72 [photon units/ 10^{18}cm^{-2}]).

fields as well as their $N(\text{HI})$ values, we calculated the DGL (plus 300 units extragalactic background) under the assumption that their galactic longitude was $\ell = 145^\circ$. This is a region where the illuminating radiation field has a much weaker gradient with latitude. The resulting slope in the DGL- $N(\text{HI})$ correlation was now 0.72 [photon units/ 10^{18} HI cm^{-2}], near the lower end of the range tabulated by Bowyer (1991). This clearly identifies the anisotropy of the illuminating radiation field as the dominant cause of the anisotropy of the DGL in the presence of a strongly forward-directed scattering phase function. The high value of the slope of the DGL/IRAS $100\mu\text{m}$ correlation found by Sasseen & Deharveng (1996) for these FAUST data is also consistent with the picture of anisotropic illumination coupled with a high value of g .

5.3. The Extragalactic Background

The present study did not permit a separate determination of the airglow and the partially attenuated extragalactic background components, except that their sum should be about 700 photon units averaged over the 14 FAUST fields. The reason for this is two-fold: We lacked a spectroscopic capability which would have been able to separate the known line emissions of the airglow from the quasi-continuous extragalactic background spectrum; and the variations in airglow intensity among different FAUST fields were large in comparison with the weak Galactic latitude dependence in the extragalactic background imposed by Galactic foreground extinction. We assumed an extragalactic component of 300 units in agreement with the determination by WP (1994) and the summary of earlier results by Paresce (1990). This produced the deduced airglow intensities listed in Table 2. After correction for Galactic foreground extinction, the extragalactic component is reduced to about 230 units for the high-latitude fields and to about 100 units for the FAUST fields with the highest $N(\text{HI})$ values leading to an average for our sample of 162 ± 46 photon units.

A discussion of the origin of the extragalactic component and the potential contributors is beyond the scope of the present paper. However, we must examine whether the assumption of an extragalactic component, anticorrelated with $N(\text{HI})$ through extinction, has a significant effect upon the final scattering characteristics derived from the DGL analysis. Repeating our analysis with the assumption that an extragalactic component in the UV is completely absent, we find that the excess intensity must then be mostly attributed to a higher airglow. The resultant albedo and phase function asymmetry are essentially unchanged, 0.43 instead of 0.45, and 0.65 instead of 0.675, respectively. Thus, should future studies reveal our assumption of 300 units for the extragalactic UV

background as inaccurate, this would not affect the validity of the present results.

On the other hand, an extragalactic component of *more* than 300 units is effectively excluded by the lower limit to the total far-UV background, including extragalactic, measured by Onaka and Kodaira (1991) who directly recorded intensities as low as 300 units at high galactic latitudes, effectively using the same bandpass. It is important to state, however, that it is not necessary to know the intensities of the airglow and the extragalactic background separately in order to determine the dust scattering properties of galactic dust, provided two conditions are met: (1) the observations must cover a sufficiently large range of galactic latitudes to allow the dependence of the measured intensity upon the HI column density to be revealed, and (2) the airglow component must be relatively constant during the observation.

6. Conclusions

We have analyzed the 140-180nm UV background intensity in 14 FAUST fields at intermediate and high Galactic latitudes after contributions from discrete sources such as stars and galaxies had been removed. We conclude the following:

(1) We confirm that a major component of the measured UV background must be of Galactic origin based on its strong correlation with $N(\text{HI})$, with $\text{cosec}|b|$, and with the IRAS $100\mu\text{m}$ background intensity. We interpret this component as DGL, produced by scattering of stellar photons by Galactic dust.

(2) The slope in the FAUST DGL- $N(\text{HI})$ correlation of 2.5 ± 0.5 [photon units/ 10^{18} HI cm^{-2}] is found to be steeper than that seen in earlier investigations in other Galactic regions. We explain this discrepancy as owing to the existence of a very strong Galactic latitude gradient in the illuminating radiation field in the FAUST region.

(3) We found our radiative transfer model capable of matching the detailed variation of the DGL intensity from one line-of-sight to another. The most important characteristic of the model responsible for this is the incorporation of the detailed anisotropy of the interstellar radiation field in the UV and its variation with z -distance from the Galactic plane.

(4) The radiative transfer analysis of the DGL component with our model resulted in a set of well-constrained scattering parameters for dust in the diffuse ISM at intermediate and high Galactic latitudes: albedo $a = 0.45 \pm 0.05$ and phase function asymmetry $g = 0.68 \pm 0.10$.

(5) The dust albedo is some 50% lower than that commonly derived for dense reflection nebulae and star forming regions. We interpret this difference as arising from a difference in size distributions with the grains in the diffuse ISM being smaller on average.

(6) A contribution of about 700 ± 200 photon units appears to be uncorrelated with Galactic lines-of-sight. We interpret this component as due to a sum of residual airglow (530 ± 190 photon units) and isotropic extragalactic background radiation (160 ± 50 photon units, after correction for Galactic extinction).

We thank Jens Petersohn for his invaluable assistance with the WP radiative transfer model during the early stages of this work. The referee, Dr. Ken Sembach, provided a number of thoughtful and constructive comments which helped to improve the presentation of this paper, and for which we are grateful. ANW and BCF acknowledge material support from NASA LTSA Grant NAGW-3168 to The University of Toledo.

Table 3.

Region	λ (nm)	a	g	R_V	Ref
NGC 7023	144,152	$\geq 0.65 \pm 0.09$	0.75 ± 0.05	~ 4	1,5
NGC 7023	130	0.62 ± 0.09	0.75 ± 0.05	~ 4	2,5
Sco OB2 Assn	177	0.64 ± 0.09	undet.	3.5	3
IC 435	156	0.75 ± 0.05	0.7 ± 0.1	5.3	4,6
Diffuse ISM	160	0.45 ± 0.05	0.68 ± 0.1	3.1	this study

References. — 1. Witt et al. 1992; 2. Witt et al. 1993; 3. Gordon et al. 1994;
 4. Calzetti et al. 1995; 5. Walker et al. 1980; 6. Snow & Witt 1989

REFERENCES

- Bohlin, R. C., Savage, B. D., & Drake, J. F. 1978, *ApJ*, 224, 132
- Boulanger, F., Abergel A., Bernard, J. -P., Burton, W. B., Désert, F. -X., Hartmann, D., Lagache, G., & Puget, J. -L. 1996, *A&A*, 312, 256
- Boulanger, F., & Pérault, M. 1988, *ApJ*, 330, 964
- Bowyer, S. 1991, *ARA&A*, 29, 59
- Bowyer, S., Sasseen, T. P., Lampton, M., & Wu, X. 1993, *ApJ*, 415, 875
- Calzetti, D., Bohlin, R. C., Gordon, K. D., Witt, A. N., & Bianchi, L. 1995, *ApJ*, 446, L97
- Carnochan, D. J., & Wilson, R. 1983, *MNRAS*, 202, 317
- Chakrabarti, S., Sasseen, T. P., Lampton, M., & Bowyer, S. 1993, *Geophys. Res. Lett.*, 20, 535
- Cleary, M. N., Haslam, C. C. T., & Heiles, C. 1979, *A&AS*, 36, 95
- Cohen, M., Sasseen, T. P., & Bowyer, S. 1994, *ApJ*, 427, 848
- Craven, P. D., & Torr, M. R. 1988, NASA Technical Memorandum 4101, NASA
- Crovisier, J. 1981, *A&A*, 94, 162
- Diplas, A., & Savage, B. D. 1994, *ApJ*, 427, 274
- FitzGerald, M. P., Stephens, T. C., & Witt, A. N. 1976, *ApJ*, 208, 709
- Fitzpatrick, E. L., & Massa, D. 1990, *ApJS*, 72, 163
- Fix, J. D., Cravens, J. D., & Frank, L. A. 1989, *ApJ*, 345, 203
- Gondhalekar, P. M. 1990, in *The Galactic and Extragalactic Background Radiation*, Proc. of IAU Symp. No. 139, S. Bowyer and C. Leinert, ed. (Dordrecht: Kluwer Acad. Publ.), 49
- Gordon, K. D., Witt, A. N., Carruthers, G. R., Christensen, S. A., & Dohne, B. C. 1994, *ApJ*, 432, 641
- Gottlieb, D. M. 1978, *ApJS*, 38, 287
- Heiles, C., & Cleary, M. N. 1979, *Austral. J. of Phys., Astroph. Suppl. No.* 47, 1

- Henry, R. C. 1991, *ARA&A*, 29, 89
- Henry, R. C., Landsman, W. R., Murthy, J., Tennyson, P. D., Wofford, J. B., & Willson, R. 1988, *The Atlas of the Ultraviolet Sky*, (Baltimore: The Johns Hopkins Univ. Press)
- Heney, L. G., & Greenstein, J. L. 1941, *ApJ*, 93, 70
- Infrared Processing and Analysis Center 1991, *CD-ROM IRAS Sky Survey Atlas*
- Jenniskens, P., & Greenberg, J. M. 1993, *A&A*, 274, 439
- Jura, M. 1979, *ApJ*, 231, 732
- Kim, S. -H., & Martin, P. G. 1996, *ApJ*, 462, 296
- Kim, S. -H., Martin, P. G., & Hendry, P. D. 1994, *ApJ*, 422, 164
- Kiszkurno, E., & Lequeux, J. 1987, *A&A*, 185, 291
- Lampton, M., Bowyer, S., & Deharveng, J. M. 1990, in *The Galactic and Extragalactic Background Radiation*, Proceedings of IAU Symposium No. 139, S. Bowyer and C. Leinert, ed., (Dordrecht: Kluwer Acad. Publ.), 449
- Lampton, M., Sasseen, T. P., Wu, X., & Bowyer, S. 1993, *Geophys. Res. Lett.*, 20, 539
- Lampton, M., Siegmund, O. H. W., Bixler, J., & Bowyer, S. 1986, *Proc. SPIE*, 627, 383
- Lequeux, J. 1990, in *The Galactic and Extragalactic Background Radiation*, Proc. of IAU Symp. No. 139, S. Bowyer and C. Leinert, ed., (Dordrecht: Kluwer Acad. Publ.), 185
- Lockman, F. J. 1984, *ApJ*, 283, 90
- Magnani, L. 1994, in *The First Symposium on the Infrared Cirrus and Diffuse Interstellar Clouds*, R. M. Cutri & W. B. Latter, ed., *ASP Conf. Ser.* 58, 161
- Magnani, L., Blitz, L., & Lada, E. A. 1986, *ApJ*, 301, 395
- Magnani, L., Hartmann, D., & Speck, B. G., 1996, *ApJS*, 106, 447
- Martin, C., & Bowyer, S. 1990, *ApJ*, 350, 242
- Martin, C., Hurwitz, M., & Bowyer, S. 1990, *ApJ*, 354, 220
- Mathis, J. S. 1993, *Rep. Prog. Phys.*, 56, 605
- Mathis, J. S., & Cardelli, J. A. 1992, *ApJ*, 398, 610

- Mattila, K. 1971, *A&A*, 15, 292
- Mattila, K. 1980a, *A&AS*, 39, 53
- Mattila, K. 1980b, *A&A*, 82, 373
- Morgan, D. H., Nandy, K., & Thompson, G. I. 1978, *MNRAS*, 185, 371
- Murthy, J., & Henry, R. C. 1995, *ApJ*, 448, 848
- Onaka, T., & Kodaira, K. 1991, *ApJ*, 379, 532
- Paresce, F. 1990, in *The Galactic and Extragalactic Background Radiation*, Proc. IAU Symp. No. 139, S. Bowyer and C. Leinert, ed., (Dordrecht: Kluwer Acad. Publ.), 307
- Sasseen, T. P., & Deharveng, J. -M. 1996, *ApJ*, 469, 691
- Sasseen, T. P., Lampton, M., Bowyer, S., & Wu, X. 1995, *ApJ*, 447, 630
- Savage, B. D., & Mathis, J. S. 1979, *ARA&A*, 17, 73
- Sembach, K. R., & Savage, B. D. 1996, *ApJ*, 457, 211
- Snow, T. P., & Witt, A. N. 1989, *ApJ*, 342, 295
- Snow, T. P., & Witt, A. N. 1995, *Science*, 270, 1445
- Snow, T. P., & Witt, A. N. 1996, *ApJ*, 468, L65
- Sofia, U. J., Cardelli, J. A., & Savage, B. D. 1994, *ApJ*, 430, 650
- Spitzer, L. 1978, *Physical Processes in the Interstellar Medium*, (New York: J. Wiley), 155
- Stark, R. 1995, *A&A*, 301, 873
- Stark, A. A., Gammie, C. F., Wilson, R. W., Bally, J., Linke, R. A., Heiles, C., & Hurwitz, M. 1992, *ApJS*, 79, 775
- van de Hulst, H. C. 1987, *A&A*, 173, 115
- van de Hulst, H. C., & de Jong, T. 1969, *Physica*, 41, 151
- Walker, G. A. H., Young, S., Fahlman, G. G., & Witt, A. N. 1980, *PASP*, 92, 411
- Witt, A. N. 1990, in *The Galactic and Extragalactic Background Radiation*, Proc. IAU Symp. No. 139, S. Bowyer and C. Leinert, ed., (Dordrecht: Kluwer Acad. Publ.), 127

- Witt, A. N., Bohlin, R. C., & Stecher, T. P. 1984, *ApJ*, 279, 698
- Witt, A. N., & Gordon, K. D. 1996, *ApJ*, 463, 681
- Witt, A. N., & Petersohn, J. K. 1994, in *The First Symposium on the Infrared Cirrus and Diffuse Interstellar Clouds*, ASP Conf. Ser. 58, R. M. Cutri and W. B. Latter, ed., 91
- Witt, A. N., Petersohn, J. K., Bohlin, R. C., O’Connell, R. W., Roberts, M. S., Smith, A. M., & Stecher, T. P. 1992, *ApJ*, 395, L5
- Witt, A. N., Petersohn, J. K., Holberg, J. B., Murthy, J., Dring, A., & Henry, R. C. 1993, *ApJ*, 410, 714
- Witt, A. N., & Stephens, T. C. 1974, *AJ*, 79, 948